(Received 5 November 2024, Accepted 12 December 2024, Scheduled 22 December 2024)

Gap-Coupled Design of Elliptical Shape Microstrip Antennas for Wideband Circular Polarized Response

Amit A. Deshmukh*, Heet Mistry, and Venkata A. P. Chavali

EXTC, SVKM's D J Sanghvi CoE, Mumbai, India

ABSTRACT: A gap-coupled design of elliptical shape microstrip antennas for wideband circularly polarized response is proposed. The wideband nature of the response is attributed to the gap-coupling between the orthogonal resonant modes on the fed and parasitic elliptical shape patches. With the total substrate thickness of $0.11\lambda_{cAR}$, the gap-coupled antenna offers the reflection coefficient bandwidth of 784 MHz (55.68%) that includes circularly polarized bandwidth for axial ratio $\leq$ 3 dB of 542 MHz (35.82%). The antenna offers a broadside radiation pattern across the bandwidth, with a peak gain larger than 10 dBi. A design methodology to realize a similar gap-coupled antenna in a different frequency range is presented that yields similar wideband results. With the obtained antenna characteristics, the proposed designs will find applications in GPS L and GSM 900 frequency bands. An experimental verification for the obtained simulated results is carried out, which provides a close agreement.

1. INTRODUCTION

Owing to the many advantages like low profile planar configuration, microstrip antenna (MSA) finds many applications in wireless communication systems [1, 2]. In wireless applications that employ line of sight mode of propagation between the transmitter and receiver, the fading of signal is a major concern. Of the many reasons that lead to a signal fading or fluctuations in the received power level, multi-path propagation plays a major role [3]. This effect arises as multiple paths for the RF signal are present between the transmitter and receiver. Different paths cause changes in the direction of polarization of transmitted wave as it arrives at the receiver antenna. If the polarization of incident wave and polarization of receiver antenna do not match, then signal loss is observed. To address this, circularly polarized (CP) antennas are selected as they can receive the signal from any orientation of the incident wave [3]. The MSA provides an optimum solution for CP response, as suitable modifications in the patch shape and the feed position, and achieves the CP response. In this line 'same' refers to 'CP characteristics

In MSA CP response is achieved either by cutting narrow slots inside the patch or by placing the open circuit stub on the patch edges [4–6], or by placing the shorting post at an appropriate position on the patch [7, 8], or by employing a modified shape of the radiation patch to excite orthogonal resonant modes [9, 10], or by cutting a resonant U-slot or a pair of rectangular slots inside the patch [11–15], or by employing MSA backed by a modified ground plane structure [16–18]. In these methods, either efficient microwave substrate or air suspended patch is used. These single patch designs offer the antenna gain of 5–8 dBi with axial ratio (AR) bandwidth (BW) of 2–6%. In the event of interference or signal jamming, dual-band CP antennas are needed. The dual-band CP response is achieved either by employing parasitic resonators [19, 20] or by embedding multiple slots inside the MSA [21]. But in dual-band CP designs, broadside gain varies over the two bands. The wideband CP designs offering AR BW $>$ 15% can cater to multiple wireless applications residing in the adjoining/nearby frequency spectrums, e.g., GPS L bands, Galileo E bands, and GSM band. To increase the AR BW and gain, either modified patch shapes with multiple resonant slots are cut inside the patch [22, 23], or multiple parasitic patches are employed in the planar or stacked layer [14, 24–29]. For wideband resonant slots cut CP designs, gain is not achieved in the broadside direction [22], or substrate thickness of nearly $0.2\lambda_{cAR}$ is needed [23]. The CP MSAs obtained using parasitic patches does not offer higher AR BW and gain in all the designs. In some of those configurations, antenna size is large, or they do offer AR BW in the range of 20%, but it does not completely cover the practical applications mentioned above, lying in the adjoining frequency bands.

In this paper, a gap-coupled design of elliptical shape MSA (EMSA) with parasitic elliptical shape patches is proposed for wideband CP response. An elliptical patch is chosen using the offset feed location, and orthogonal resonant modes are easily excited on the fed patch. Further resonant modes on the elliptical patch are similar in distribution to that of the circular MSA (CMSA) [1, 2]. Due to this, the fed elliptical patch will provide rejection to the harmonic frequency as supplied by the input radio frequency (RF) source. Initially, with the total substrate thickness of 2.16 cm ($0.097\lambda_{cAR}$), EMSA excited using the offset position of the proximity feed provides CP response. It yields simulated reflection coefficient (S_{11}) ≤ -10 dB BW of 780 MHz (53.6%) that includes AR BW for $\leq$ 3 dB of 86 MHz (6.52%). As the paper deals with a CP design, electrical thick-

* Corresponding author: Amit A. Deshmukh (amitdeshmukh76@gmail.com).

ness of the substrate is expressed in terms of the wavelength (λ_{cAR}) at the center frequency of AR BW. A single elliptical patch yields a broadside radiation pattern with a peak gain of 8.1 dBi. To enhance the AR BW and gain, simpler gap-coupled technique is employed, and elliptical shape patches were gap-coupled along x and y co-ordinate axes of the fed EMSA. To obtain a symmetrical gap-coupled design, patches were coupled along both the axes. A parametric study was carried out to optimize the AR BW. An optimum gap-coupled design of EMSAs with patches along x- and y-axes offers S_{11} BW of 784 MHz (55.68%), which includes AR BW of 542 MHz (35.82%). The antenna offers broadside radiation characteristics across the entire S_{11} BW with a peak gain more than 10 dBi. The gap-coupled design offers almost six times increase in % AR BW with nearly 3 dBi increase in the peak gain. Design methodology to realize a similar gap-coupled wideband CP antenna in a specific frequency spectrum is presented. The antenna is designed using the same to cover the entire GPS L band (L1, L2, L3, L5) and GSM 900 MHz frequency band. The redesigned wideband CP antenna shows similar AR BW and gain characteristics, and a single design caters to the complete frequency spectrum of the said application. To highlight the technical novelty in the proposed work, detailed comparison of the proposed design against reported narrow and wideband CP designs is presented. It reflects that, in terms of the technique used, antenna volume, AR BW, and peak gain, the proposed design offers an optimum solution. In the proposed work, although the reported method of parasitic patches is employed for the BW improvement, present work initially selects an elliptical patch that provides harmonic frequency rejection for the input RF source. Further for the antenna volume of the gap-coupled structure, the achieved AR BW is more than 32%, which is substantially large as against the reported gap-coupled CP antennas. Also, with this BW, a single antenna can cater to many frequency bands of given wireless applications. These are all the new contributions in the proposed gap-coupled design. The gap-coupled antenna response is initially optimized using CST software [31], followed by experimental verifications. In the experimentation, RF instruments namely ZVH-8, FSC 6, and SMB 100 A were used. A good agreement is obtained between the simulated and measured results.

2. GAP-COUPLED DESIGN OF EMSA WITH PARASITIC EMSAS

Gap-coupled design of proximity fed EMSA with parasitic EMSAs placed along the two co-ordinate axes is shown in Figs. 1(a) and (b). The design initiates an elliptical patch fed using the proximity strip. The EMSA is fabricated on an FR4 substrate ($\varepsilon_r = 4.3$, $h = 0.16$ cm), which is suspended above the ground plane using an air gap of thickness h_a cm. A square proximity strip of length L_s cm is placed below the patch at thickness of h_s cm and for the co-ordinates as x_f, y_f cm, as mentioned in Figs. 1(a) and (b). For the total substrate thickness of 2.16 cm ($h_a = 2.0$ cm) and TM_{11} mode frequency of 1200 MHz, patch radius 'a' is calculated by using Equation (1). Resonant field distributions in elliptical patch are similar to that of circular MSA. Hence, the frequency equation for circular patch is used.

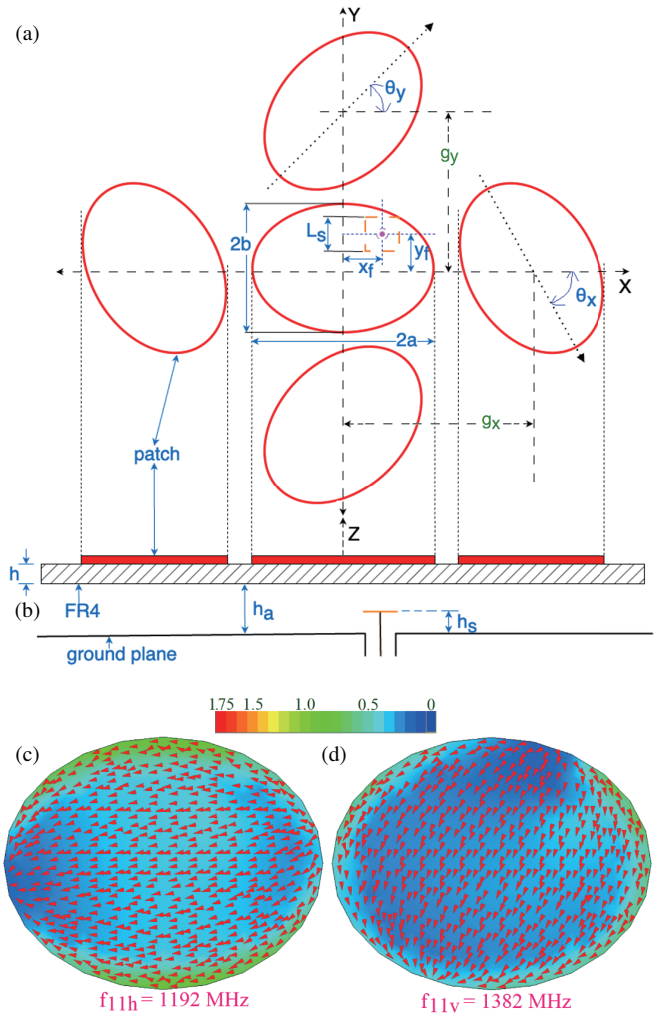

FIGURE 1. (a), (b) Proximity fed EMSA gap-coupled with parasitic EMSAs, (c), (d) average and vector surface current distribution at orthogonal modes for proximity fed EMSA.

For the elliptical patch, this TM_{11} mode frequency is for the patch radius along horizontal axis (TM_{11h}) as mentioned in Fig. 1(a). The effective dielectric constant (ε_{re}) for the above substrate parameters is calculated by using Equation (2).

$$a = \left(K_{mn}c/2f_{11}\pi\sqrt{\varepsilon_{re}}\right) - 0.9\,(h + h_a) \tag{1}$$

$$\varepsilon_{re} = \frac{\varepsilon_r\,(h + h_a)}{h + h_a\varepsilon_r} \tag{2}$$

where $K_{mn} = 1.84118$, $c = 30$, frequency is specified in GHz in the above equation, and thus 'a' is calculated in cm.

The radius 'a' is calculated to be 5.2 cm. By employing parametric study for the orthogonal radius 'b' of the elliptical patch, which governs TM_{11v} mode frequency and the proximity feed parameters, EMSA is optimized for the CP response. The CP response in EMSA is attributed to the optimum inter-spacing between the TM_{11h} and TM_{11v} resonant modes at which surface currents are orthogonal as mentioned in Figs. 1(c) and (d). Antenna dimensions in the elliptical patch CP design are $b = 4.1$, $h_s = 1.8$, $L_s = 1.5$, $x_f = 2.4$, $y_f = 2.2$ cm.

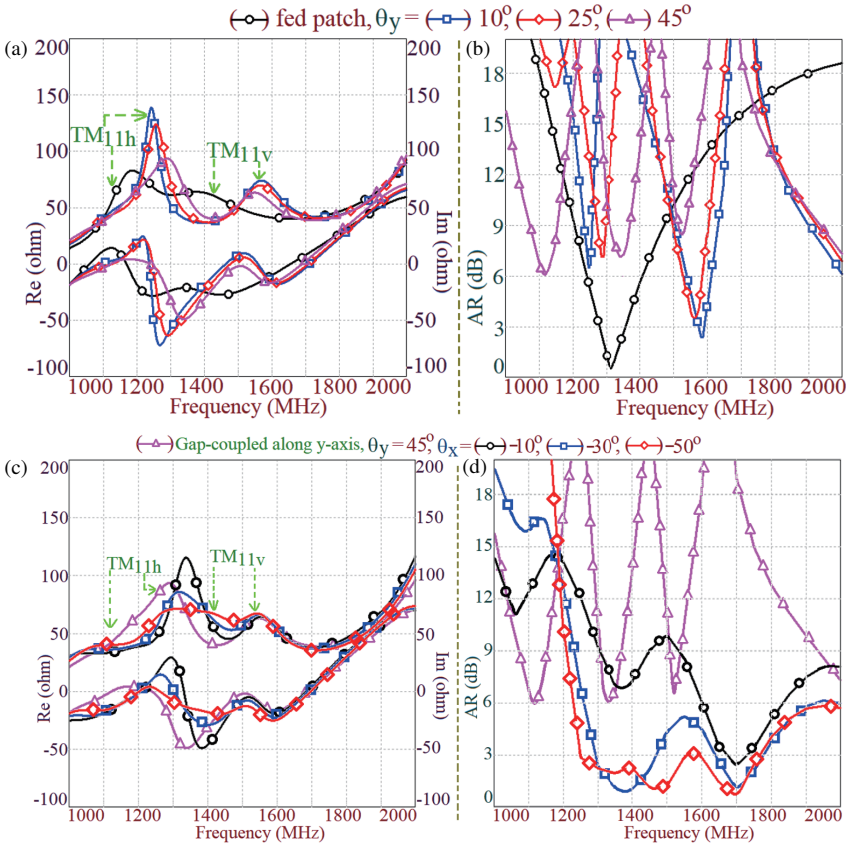

FIGURE 2. (a)–(d) Resonance curve and AR plots showing variations in orthogonal mode frequencies and respective AR values for the gap-coupled design of EMSAs along y and x-axis.

The EMSA yields simulated S_{11} BW of 780 MHz (53.6%), which includes AR BW of 86 MHz (6.52%). The antenna offers broadside radiation pattern with a peak gain of 8.1 dBi. To increase the AR BW and gain of the elliptical patch, multi-resonator gap-coupled design is used, and elliptical patches of same radius as that of fed patch are coupled along the x- and y-axes as mentioned in Fig. 1(a). The parameters that control the AR BW in the gap-coupled design are frequencies of the orthogonal modes across all the patches, angular separation of the parasitic patch with respect to fed patch axis, and the spacing of parasitic patch with reference to the fed elliptical patch. As orthogonal modes need to be excited on the parasitic patches, angular displacement of parasitic patch with reference to fed patch axis is needed.

For the same patch radius in all the gap-coupled and fed EMSAs, initially parametric study for variation in angular separation between the fed and parasitic patches is carried out. The simulated resonance curve and AR plots for them are shown in Figs. 2(a)–(d). Initially, patches only along y-axis were considered, and later patches along x-axis were added in the gap-coupled configurations. In Figs. 2(a) and (b), plots are shown for single patch and with patches added along y-axis, which are provided with an angular displacement of angle θ_y, with reference to the fed patch axis. With the addition of patches along y-axis, orthogonal resonant modes are added in the gap-coupled design, but configuration yields dual or triple band CP response, as noted from the AR curve. The objective of this study is to provide a wideband solution, and hence, individual multi-band CP response, which could have been obtained with the patches along y-axis, was not persuaded further. In addition to the angular variation, parametric variations were also carried out against variation in parasitic patch radius and spacing of the same with respect to fed patch. But none of these variations resulted in wideband CP characteristics supported with an appropriate impedance matching. In the gap-coupled design with patches along y-axis and for $\theta_y = 45°$, identical radius elliptical patches were added along the x-axis. As the frequencies of the patches along x-axis are not different, additional resonant peaks are not observed in the resonance curve, but an impedance variation at them is noted as shown in Figs. 2(c) and (d). The impedance at the resonant modes decreases below 50 Ω, and the AR value decreases below 3 dB over a wide frequency range, with an increase in angle θ_x for the patches along x-axis.

In the above plots, positive value of the angle mentioned indicates the rotation in anticlockwise direction, whereas negative value of the angle indicates that rotation is in the clockwise direction. As noted from the above plots, for equal patch radius and $\theta_y = 45°$, $\theta_x = -50°$, wideband CP response for AR less than 3 dB is achieved.

For the optimum CP design with patches along x- and y-axes, various antenna parameters are $h_a = 2.0$, $h = 0.16$, $a = 5.2$, $b = 4.1$, $g_x = 11.0$, $g_y = 9.3$, $h_s = 1.8$, $L_s = 1.5$, $x_f = 2.4$, $y_f = 2.2$ cm, and results for them are provided in Figs. 3–

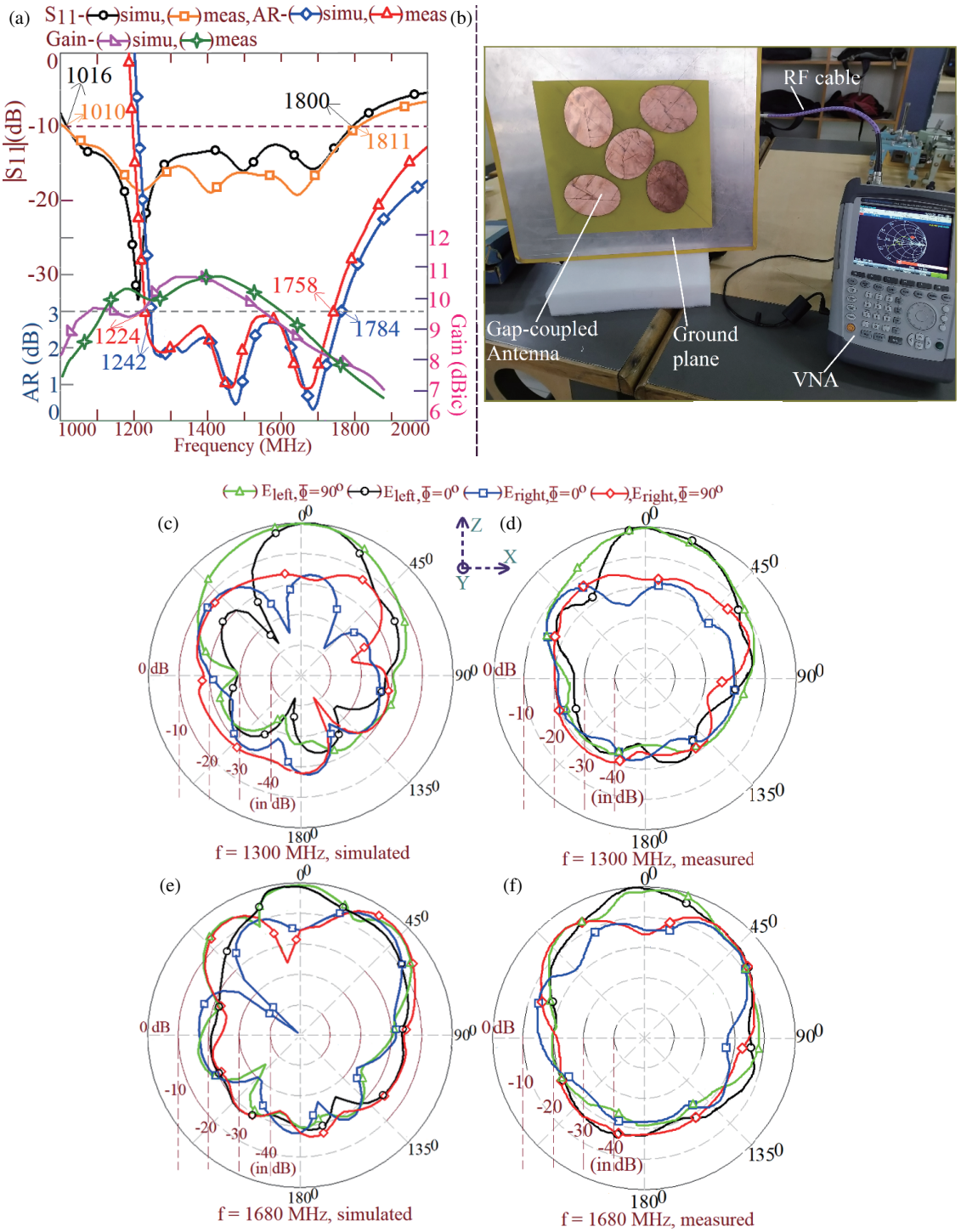

FIGURE 3. (a) S_{11} & AR BW and gain plots, (b) S_{11} BW measurement setup, (c)–(h) E-field polarization plots over the AR BW, for gap-coupled variation of EMSAs along x and y-axis.

5. A square ground plane of side length 50 cm is used in the simulation and measurement, and the antenna is fed using an N-type connector of 0.32 cm inner wire diameter.

The simulated and measured BWs for $S_{11} \leq -10$ dB are 784 MHz (55.68%) and 801 MHz (56.78%), respectively. The antenna offers simulated and measured AR BWs of 542 MHz (35.82%) and 534 MHz (35.81%), respectively, and it offers the peak gain of more than 10.5 dBi. Over most of the S_{11} and AR BW, the antenna gain remains above 6 dBi. Polar radiation pattern plots showing right-hand CP (RHCP) and left-hand CP (LHCP) fields towards the band edge frequencies of the AR BW shows the dominance of LHCP radiation. The RHCP component is more than 10 dB lower than the LHCP component. This shows that antenna radiates LHCP wave. With respect to the observer, time varying surface current distribution rotates in clockwise direction. But with respect to the antenna as a radi-

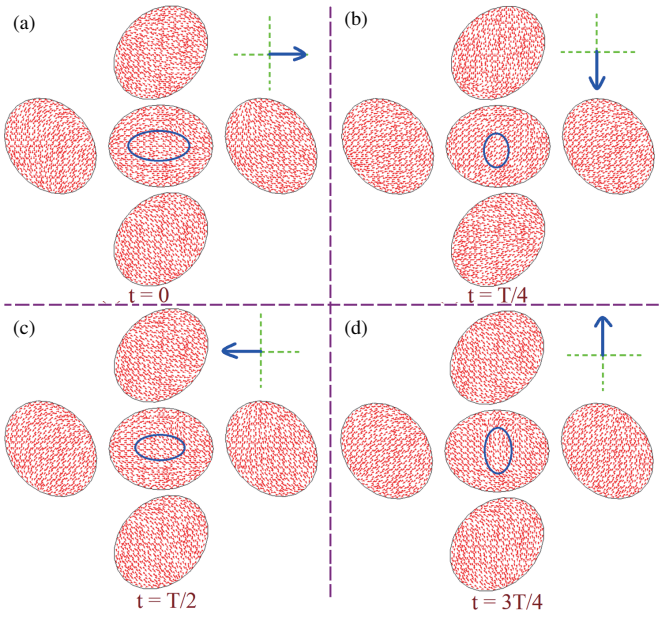

FIGURE 4. (a)–(d) Time varying surface current distribution at the center frequency of the AR BW for gap-coupled design of proximity fed EMSAs along x and y-axis.

ator, the same will appear anti-clockwise in the direction, thus realizing LHCP response. The orthogonal field magnitudes and their phase plots as picked up by the orthogonal probes in the far-field region are shown in Fig. 5(a). As can be noted, over a wide range of frequencies, E_x and E_y plots are nearly the same in magnitude. Over the same range, Φ_y either leads Φ_x by 90° or lags by 270°. With reference to the antenna as a radiator, this phase difference gives LHCP signal. Thus, simulated and measured field polarization plots, time varying surface current distribution and orthogonal E-field magnitude and their phase plots shows the wideband nature of the CP response offered by the gap-coupled antenna. Radiation pattern, AR BW and gain measurement setup is shown in Fig. 5(b). In these measurements, reference wideband high gain horn antennas are used. A minimum far-field distance between the antenna under test (AUT) and reference horn antenna is calculated with reference to the highest frequency of the S_{11} BW. As seen from the setup, around the desk and in the line of sight of the measurement, metallic objects are not present. The distance of surrounding walls with reference to the central measurement desk is more than eight times of the operating wavelength, calculated with reference to the lowest frequency of S_{11} BW. All these details ensure the measurement in laboratory as close as possible to the ideal environment present in the anechoic chamber. The radiation pattern is measured in far field in the two polarizations, i.e., vertical and horizontal. Further, by using the conversion equations [32], right- and left-hand field components are evaluated. For better accuracy, three-antenna method is used in the gain measurement.

A gap-coupled CP configuration with EMSA coupled only along x-axis was also studied. This gap-coupled antenna does not give wideband CP characteristics, and hence their results are not discussed. To explain the generation of wideband CP response with the addition of parasitic patches along x- and y-axes, surface current distributions for single elliptical patch and gap-coupled patches are studied as shown in Figs. 6(a)–(e). The surface current distribution is shown at a single frequency over the AR BW at a given instant of time for the patches either along x- or y-axis, whereas the same is shown at given time instant at two frequencies over the AR BW in the configuration with patches gap-coupled along x- and y-axes. With the addition of parasitic patches either along x- or y-axis, orthogonality of surface current components over the effective antenna aperture is not achieved, and due to this wideband CP response with patches along x or y-axis is not obtained. Against this, with patches along x- and y-axes together, surface current orthogonality across the elliptical patches is maintained over a wide frequency range that achieves a wideband CP response. The antenna size does increase with the patches along x- and y-axes together, but a substantial increase in the AR BW and peak gain is noted.

3. DESIGN METHODOLOGY FOR WIDEBAND GAP-COUPLED CP EMSA

The proposed gap-coupled design of proximity fed EMSA discussed above yields more than 32% of AR BW. This value is quite large as the said BW can cater to multiple adjoining wireless applications. In this regard, this section presents the design methodology to realize a similar gap-coupled antenna as per the specific wireless applications. In addition to the resonance frequency formula for circular (elliptical) patch, various frequency and dimensional relations, which are present in the above gap-coupled design are used in the design methodology. The methodology is initiated by specifying the center frequency of the AR BW, f_{cAR}. This frequency can be as per any given wireless application. Using the frequency relation as mentioned in (3), TM_{11h} mode frequency of the proximity fed elliptical patch is calculated. The total substrate thickness for the gap-coupled antenna is calculated using Equation (4).

$$f_{11h} = {}^{f_{cAR}}\!/_{1.274} \tag{3}$$

$$h_t = 0.0874\left({}^{30}\!/_{f_{11h}\sqrt{\varepsilon_{re}}}\right) \tag{4}$$

This thickness (h_t) equals air gap thickness plus the substrate thickness. Initially, air gap thickness is not available, and thus the value of ε_{re} is not available to start with. Hence, the initial approximation of $\varepsilon_{re} = 1.06$ is considered. This approximation is based on the value of ε_{re} as present in the above optimum design, for the mentioned substrate parameters. From Equation (4), h_t is obtained, and for FR4 substrate ($h = 0.16$ cm), h_a is calculated as $h_a = h_t - h$. In most of the cases, this will yield a non-integer and thus a practically not realizable number. Hence, this value is rounded off to the nearest integer number for which air gap thickness is realizable. Later for this air gap and substrate parameters, ε_{re} is recalculated using Equation (2), and it is used in all further calculations. The elliptical patch radius along the horizontal axis 'a' is calculated by using Equation (5), and further, patch radius along the vertical axis is selected as $b = 0.79a$. The radius of all the parasitic patches is the same as that of the fed EMSA. Along the x- and

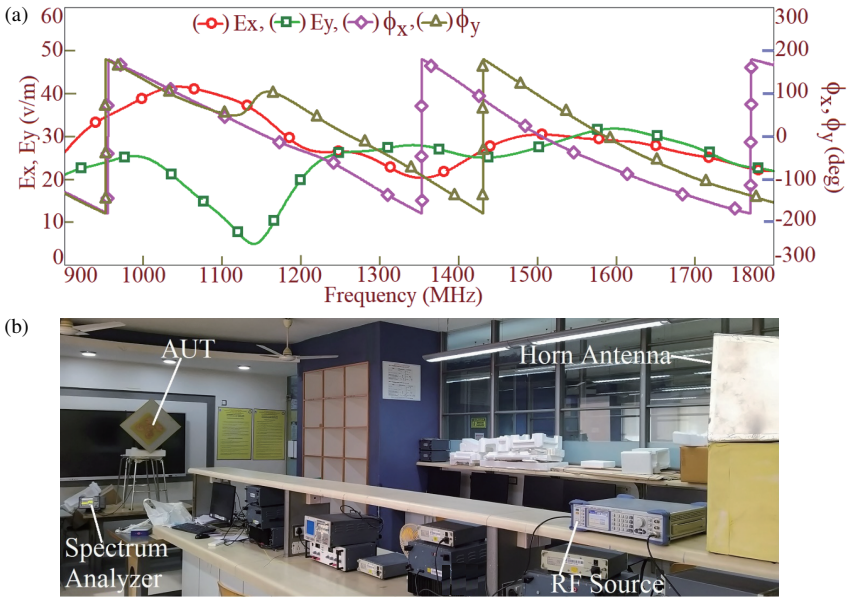

FIGURE 5. (a) E-field magnitude and phase plots and (b) gain measurement setup for gap-coupled design of proximity fed EMSAs along x and y-axis for wideband CP response.

y-axes, parasitic EMSAs are placed at a distance of $5.093h_t$ and $4.305h_t$, respectively, with respect to the fed EMSA. The proximity strip parameters are selected as $h_s = 0.073\lambda_{g11h}$, $L_s = 0.073\lambda_{g11h}$, $x_f = 0.073\lambda_{g11h}$, $y_f = 0.073\lambda_{g11h}$. Here, λ_{g11h} is the wavelength at TM_{11h} mode frequency as calculated using Equation (6). The units of frequency and antenna dimension mentioned in all the equations are in GHz and cm, respectively

$$a = \left(30K_{mn}/2f_{11h}\pi\sqrt{\varepsilon_{re}}\right) - 0.95\,(h + h_a) \quad (5)$$

$$\lambda_{g11h} = 30/f_{11h}\sqrt{\varepsilon_{re}} \quad (6)$$

Using the above design methodology, gap-coupled configuration of EMSAs is designed to cover GSM frequency band (820–1120 MHz) with the center frequency around 980 MHz and GPS L band (1160–1590 MHz) with center frequency around 1370 MHz. An air suspended FR4 substrate is used in both the designs. For the GSM band, various antenna parameters are $h_a = 3.2$, $h = 0.16$, $a = 8.0$, $b = 6.3$, $g_x = 17.1$, $g_y = 14.5$, $h_s = 2.8$, $L_s = 2.35$, $x_f = 3.7$, $y_f = 3.4$ cm, and results for them are provided in Figs. 7(a) and (b).

The gap-coupled proximity fed EMSA offers simulated and measured S_{11} BW of 477 MHz (52.16%) and 497 MHz (54.53%), respectively. The CP AR BWs for ≤ 3 dB observed in the simulation and measurement are 293 MHz (29.73%) and 296 MHz (30.3%), respectively. The antenna offers a broadside radiation pattern across the complete AR BW with a peak gain of 10 dBi. The center frequency of AR BW observed in the simulation is 985 MHz, which is close to the initial selected frequency of 980 MHz. For the GPS L-band, various antenna dimensions are $h_a = 2.2$, $h = 0.16$, $a = 5.7$, $b = 4.5$, $g_x = 12.0$, $g_y = 10.1$, $h_s = 2.0$, $L_s = 1.65$, $x_f = 2.65$, $y_f = 2.4$ cm. Proximity fed gap-coupled EMSA for GPS L-band offers simulated and measured S_{11} BW of 721 MHz (56.88%) and 732 MHz (57.05%), respectively. The AR BWs observed in the simulation and measurement are 470 MHz (33.93%) and 482 MHz (34.03%), respectively. The center frequency of the AR BW observed in the simulated result is 1385 MHz, which is very close to the initially selected value of 1370 MHz. This antenna covers the entire GPS L-bands, i.e., L1, L2, L3, and L5. Gap-coupled antenna covering GPS L frequency bands offers broadside radiation pattern with a peak gain of more than 10 dBi. With the achieved AR BW of more than 30% and unlike the reported wideband gap-coupled CP antennas, the proposed design can cover many of the adjoining frequency spectrums of the same wireless application and thus provides a single antenna solution. The antenna gain is also large enough to cater to the practical application requirements. The following section provides a detailed comparative analysis against the reported CP MSAs to show the technical novelty in the proposed configuration.

4. RESULTS DISCUSSION AND COMPARATIVE ANALYSIS

This section compares the performance of gap-coupled proximity fed EMSA against the reported narrow and wideband CP MSAs. The comparison is presented for the measured S_{11} and AR BW against the peak gain and the antenna volume, i.e., patch area (A_P) and total substrate thickness (h_t). The tabular comparison is presented in Table 1.

The CP designs discussed in [5–8, 10] are optimized on a thinner but efficient microwave substrate. Due to this, MSA offers narrow AR BW. The modified triangular patch design discussed in [9] employs overlap patches and thicker substrate but offers only 6% of AR BW. The resonant slots cut design for CP response is the optimum configuration as single patch

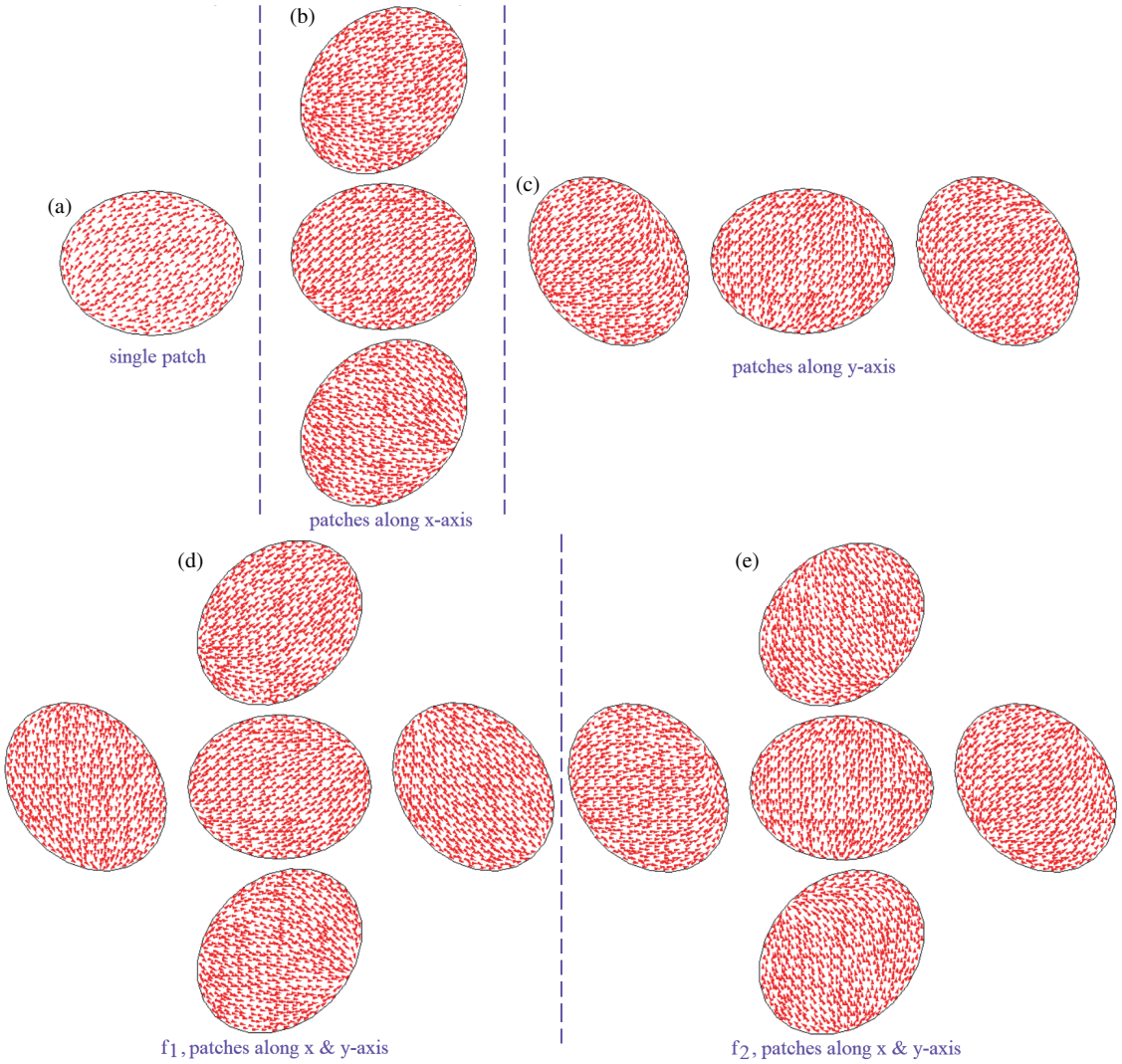

FIGURE 6. (a)–(e) Surface current distribution over the AR BW for single elliptical patch and gap-coupled variation of elliptical patches.

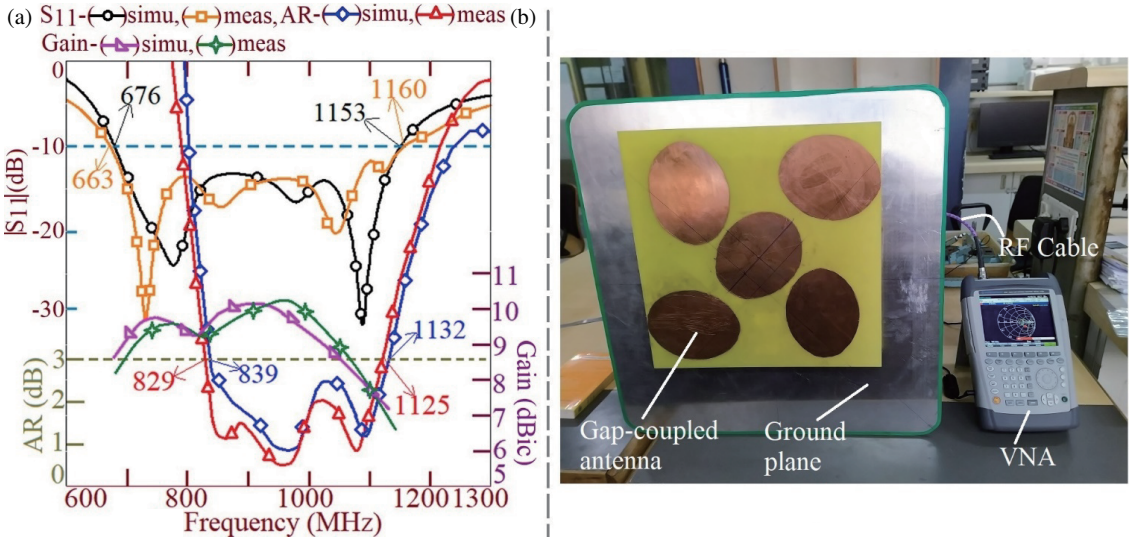

FIGURE 7. (a) S_{11} & AR BW and gain plots and (b) S_{11} BW measurement setup with fabricated antenna for proximity fed EMSAs design to cover GSM 900 MHz frequency band.

TABLE 1. Comparison for the proposed wideband CP EMSA against the reported configurations.

MSA shown in	Meas. BW (MHz, %)	AR BW (MHz, %)	Peak Gain (dBi)	Area (A_P/λ^2_{cAR})	Substrate thickness (h_t/λ_{cAR})
Figs. 1(a), (b)	801, 56.78	534, 35.81	10.7	1.225	0.11
Ref. [5]	27, 1.71	10, 0.63	5.4	0.14	0.03
Ref. [6]	85, 3.41	23, 0.93	3.87	0.4	0.02
Ref. [7]	350, 6.8	34, 1.33	10.3	0.241	0.04
Ref. [8]	67, 2.72	16, 0.653	7.6	0.51	0.04
Ref. [9]	653, 54	76, 6.12	8.5	0.23	0.11
Ref. [10]	35, 2.2	8, 0.5	3.9	0.44	0.02
Ref. [11]	260, 11.2	90, 3.9	9.0	0.2	0.077
Ref. [13]	230, 9.27	230, 9.27	8.3	0.23	0.08
Ref. [14]	710, 29.64	480, 20.08	11.5	>2.5	0.095
Ref. [15]	810, 35	130, 5.3	9.0	0.21	0.1
Ref. [16]	30, 1.9	6, 0.4	2.3	0.215	0.05
Ref. [18]	162, 5.71	60, 2.14	5.5	0.233	0.02
Ref. [19]	38, 1.8	9, 0.4	8.4	0.16	0.036
Ref. [20]	500, 20.41	400, 16.6	1.9	0.19	0.02
Ref. [21]	2000, 37.66	550, 11.74	7.0	0.4	0.12
Ref. [22]	2000, 40	1000, 19	7.5	0.65	0.12
Ref. [23]	1570, 28.11	1160, 21.05	8.0	0.15	0.183
Ref. [24]	180, 6	100, 3.3	2.7	0.82	0.03
Ref. [25]	80, 4.1	30, 1.54	8.4	2.362	0.05
Ref. [26]	330, 9.36	250, 7.13	7.75	0.67	0.052
Ref. [27]	300, 15.2	160, 8.2	7.0	0.14	0.067
Ref. [28]	1047, 42.5	709, 28	7.9	0.41	0.12
Ref. [29]	1203, 49.29	488, 20.11	7.5	0.32	0.14
Ref. [30]	3080, 63.3	3040, 63.7	17.77	6.2	0.101

configuration with substrate thickness in the range of $0.08\lambda_g$ offers AR BW of 5–6% with a broadside gain of 7–8 dBi [11–15]. Against this in the proposed work, simpler gap-coupling technique has been employed which offers substantially higher AR BW than resonant slot cut CP configurations. The modified ground plane design optimized on an efficient microwave substrate offers AR BW $\leq$ 2% [16, 18]. The dual-band design employing multiple patches and excited using a proximity strip offers lower AR BW [19]. The AR BW is large with smaller antenna volume for the configuration discussed in [20]. However, it has very low gain. Dual band and wideband CP configurations discussed in [21, 22] do not offer circularly polarized characteristics in the broadside direction and thus pose alignment problem with respect to the incident wave. Further, the designs discussed in [21, 22] are complex in designing as against the proposed design that employs simple gap-coupled equal radius patches. The triple mode U-slot cut antenna discussed in [23] does offer larger AR BW while using a single patch. However, in the reported work, an explanation for the patch/slot modes, which yield additional 10% AR BW as against the conventional unequal length U-slot cut CP design, is not discussed. Also, the study in [23] does not provide any design formulation for single patch wide AR BW CP design. In spite of using multiple resonators for the configurations discussed in [24–27], AR BW is lower than the proposed design. In the proposed antenna, as radii of the patches are equal along two axes, only two sets of resonator patches offering orthogonal modes are present. With this and proximity feeding, the proposed design offers higher AR BW than the reported multi-resonator CP antennas. The wideband CP designs discussed in [28, 29] employ a similar gap-coupled technique for AR BW improvement. But for equivalent substrate thickness, they offer lower AR BW than the proposed design. The patch area appears smaller in the designs discussed in [28, 29] than the proposed gap-coupled antenna. This is because the designs discussed in [28, 29] were optimized in higher frequency range. Against the reported configurations compared in Table 1, antenna area of the proposed design is large. This attributed to the use of air suspended configurations while using lossy substrate, as against the efficient but costly substrate used in reported CP designs. Further, parasitic patches are used along both the axes of the fed patch in the proposed antenna, which increases patch size but also adds to the AR BW and gain.

To summarize, proposed design employs simpler gap-coupled technique for enhancing the AR BW while using elliptical patches. On substrate thickness around $0.11\lambda_{cAR}$,

it offers nearly 35% of AR BW with a peak gain of 10.7 dBi. With this AR BW, a single antenna can be used to cater to multiple wireless application bands occupying adjoining spectrums. The redesigned configurations for couple of such applications are presented above. While using a simple gap-coupled design, none of the reported work provides this AR BW solution that caters to multiple frequency bands for a given application. The patch area while using the gap-coupled design has been increased, but it achieves larger AR BW and gain. The configuration that employs multiple patches in the planar or stacked layer or the array designs offers large AR BW and gain [30]. Against them, the proposed design offers lower AR BW but requires less number of patches, and thus offers simpler design solution for the given application. The design methodology is also presented, which is useful in realizing a similar antenna so as to cater to specific wireless application. Thus, a simpler gap-coupled design offering 35% of AR BW with a peak gain of more than 10.5 dBi is the novelty in the proposed work as compared with the reported configurations.

5. CONCLUSIONS

A wideband CP design, employing proximity fed elliptical patches in the gap-coupled configuration is proposed. The design with patches along the two co-ordinate axes offers optimum result. With the substrate thickness of $0.11\lambda_{cAR}$, the proposed antenna offers 35% of AR BW, which is completely inside the S_{11} BW of 56.78%. The antenna shows a broadside radiation pattern with a peak gain of 10.7 dBi. Across the complete S_{11} BW, the antenna gain remains above 6 dBi, which is an appreciably large gain from practical applications. The design methodology is presented that helps in realizing similar configurations as per specific wireless applications. With 35% of AR BW, the proposed design offers a single antenna solution where it can cater to multiple wireless application bands lying in the adjoining frequency spectrums. With the obtained antenna characteristics, the proposed design can find applications in GSM 900 and GPS L band applications.

REFERENCES

[1] Wong, K.-L., *Compact and Broadband Microstrip Antennas*, John Wiley & Sons, 2004.

[2] Garg, R., *Microstrip Antenna Design Handbook*, Artech House, 2001.

[3] Balanis, C. A., *Antenna Theory: Analysis and Design*, John Wiley & Sons, 2015.

[4] Kumar, G. and K. P. Ray, *Broadband Microstrip Antennas*, Artech House, 2002.

[5] Wang, M.-S., X.-Q. Zhu, Y.-X. Guo, and W. Wu, "Compact circularly polarized patch antenna with wide axial-ratio beamwidth," *IEEE Antennas and Wireless Propagation Letters*, Vol. 17, No. 4, 714–718, 2018.

[6] Ray, M. K., K. Mandal, and N. Nasimuddin, "Low-profile circularly polarized patch antenna with wide 3 db beamwidth," *IEEE Antennas and Wireless Propagation Letters*, Vol. 18, No. 12, 2473–2477, 2019.

[7] Zhang, X. and L. Zhu, "High-gain circularly polarized microstrip patch antenna with loading of shorting pins," *IEEE Transactions on Antennas and Propagation*, Vol. 64, No. 6, 2172–2178, 2016.

[8] Zhang, X., L. Zhu, and N.-W. Liu, "Pin-loaded circularly-polarized patch antennas with wide 3-db axial ratio beamwidth," *IEEE Transactions on Antennas and Propagation*, Vol. 65, No. 2, 521–528, 2017.

[9] Deshmukh, A. A. and K. P. Ray, "Circularly polarized designs of modified isosceles triangular microstrip antennas," *Engineering Reports*, Vol. 2, No. 10, e12250, 2020.

[10] Shi, Y. and J. Liu, "A circularly polarized octagon-star-shaped microstrip patch antenna with conical radiation pattern," *IEEE Transactions on Antennas and Propagation*, Vol. 66, No. 4, 2073–2078, 2018.

[11] Lee, K. F., K. M. Luk, W. C. Mok, and P. Nayeri, "Single probe-fed circularly polarized patch antennas with u-slots," *Microwave and Optical Technology Letters*, Vol. 53, No. 6, 1245–1253, 2011.

[12] Chen, Y. and C.-F. Wang, "Characteristic-mode-based improvement of circularly polarized u-slot and e-shaped patch antennas," *IEEE Antennas and Wireless Propagation Letters*, Vol. 11, 1474–1477, 2012.

[13] Khidre, A., K. F. Lee, F. Yang, and A. Elsherbeni, "Wideband circularly polarized e-shaped patch antenna for wireless applications," *IEEE Antennas and Propagation Magazine*, Vol. 52, No. 5, 219–229, 2010.

[14] Kovitz, J. M., H. Rajagopalan, and Y. Rahmat-Samii, "Design and implementation of broadband mems rhcp/lhcp reconfigurable arrays using rotated e-shaped patch elements," *IEEE Transactions on Antennas and Propagation*, Vol. 63, No. 6, 2497–2507, 2015.

[15] Kovitz, J. M., H. Rajagopalan, and Y. Rahmat-Samii, "Circularly polarised half e-shaped patch antenna: A compact and fabrication-friendly design," *IET Microwaves, Antennas & Propagation*, Vol. 10, No. 9, 932–938, 2016.

[16] Wei, K., J. Y. Li, L. Wang, R. Xu, and Z. J. Xing, "A new technique to design circularly polarized microstrip antenna by fractal defected ground structure," *IEEE Transactions on Antennas and Propagation*, Vol. 65, No. 7, 3721–3725, 2017.

[17] Wei, K., B. Zhu, and M. Tao, "The circular polarization diversity antennas achieved by a fractal defected ground structure," *IEEE Access*, Vol. 7, 92 030–92 036, 2019.

[18] Ambekar, A. G. and A. A. Deshmukh, "Low profile design of regular shape microstrip antennas backed by fractal slots cut ground plane for circular polarized response," *Progress In Electromagnetics Research C*, Vol. 129, 203–219, 2023.

[19] Liang, Z.-X., D.-C. Yang, X.-C. Wei, and E.-P. Li, "Dual-band dual circularly polarized microstrip antenna with two eccentric rings and an arc-shaped conducting strip," *IEEE Antennas and Wireless Propagation Letters*, Vol. 15, 834–837, 2015.

[20] Kumar, P., S. Dwari, R. K. Saini, and M. K. Mandal, "Dual-band dual-sense polarization reconfigurable circularly polarized antenna," *IEEE Antennas and Wireless Propagation Letters*, Vol. 18, No. 1, 64–68, 2019.

[21] Deshmukh, A. A. and A. A. Odhekar, "Dual band circularly polarized modified ψ-shape microstrip antenna," *Progress In Electromagnetics Research C*, Vol. 115, 161–174, 2021.

[22] Mondal, T., S. Maity, R. Ghatak, and S. R. B. Chaudhuri, "Design and analysis of a wideband circularly polarised perturbed psi-shaped antenna," *IET Microwaves, Antennas & Propagation*, Vol. 12, No. 9, 1582–1586, Jul. 2018.

[23] Zeng, J., X. Liang, L. He, F. Guan, F. H. Lin, and J. Zi, "Single-fed triple-mode wideband circularly polarized microstrip antennas using characteristic mode analysis," *IEEE Transactions on Antennas and Propagation*, Vol. 70, No. 2, 846–855, Feb. 2022.

[24] Lin, J.-F. and Q.-X. Chu, "Enhancing bandwidth of cp microstrip antenna by using parasitic patches in annular sector shapes to control electric field components," *IEEE Antennas and Wireless Propagation Letters*, Vol. 17, No. 5, 924–927, May 2018.

[25] Chen, J., C. Jin, B. Zhang, and Z. Shen, "Combined triangle quarter-wavelength patches and their application to high-gain cp antenna," *IEEE Antennas and Wireless Propagation Letters*, Vol. 19, No. 1, 104–108, Jan. 2019.

[26] Wu, Q.-S., X.-Y. Tang, X. Zhang, L. Zhu, G. Zhang, and C.-B. Guo, "Circularly-polarized patch antennas with enhanced bandwidth based on capacitively coupled orthogonal patch radiators," *IEEE Open Journal of Antennas and Propagation*, Vol. 4, 472–483, 2023.

[27] Cheng, G., B. Huang, Z. Huang, and L. Yang, "A high-gain circularly polarized filtering stacked patch antenna," *IEEE Antennas and Wireless Propagation Letters*, Vol. 22, No. 5, 995–999, 2023.

[28] Deshmukh, A. A., A. Doshi, and A. A. Odhekar, "Gap-coupled designs of star shape microstrip antennas for dual band and wide band circular polarized response," *International Journal of RF and Microwave Computer-Aided Engineering*, Vol. 29, No. 5, e21664, 2019.

[29] Deshmukh, A. A., V. A. P. Chavali, and A. G. Ambekar, "Circularly polarized gap-coupled designs of modified square microstrip antennas for wlan and bluetooth applications," *Progress In Electromagnetics Research C*, Vol. 138, 233–246, 2023.

[30] Verma, A., M. Arrawatia, and G. Kumar, "High gain wideband circularly polarized microstrip antenna array," *IEEE Transactions on Antennas and Propagation*, Vol. 70, No. 11, 11 183–11 187, 2022.

[31] CST Software Version 2019.

[32] Toh, B. Y., R. Cahill, and V. F. Fusco, "Understanding and measuring circular polarization," *IEEE Transactions on Education*, Vol. 46, No. 3, 313–318, Aug. 2003.